

# Chapter 9

## Defects introduced in antimony-doped germanium during metallization by electron beam deposition

### 9.1 Introduction

To completely characterize defects in semiconductor materials, defects introduced by light and heavy particles should be investigated. Unlike high energy electrons which introduce well spaced vacancies and interstitial distributed evenly throughout the sample, which then diffuse to form simple stable defects at room temperature, heavy particles introduce densely populated vacancy-rich and interstitial rich regions with the interstitials concentrated at the near-end regions of the ion range, leading to complex defect formation [1]. Heavy ions (ions larger than protons or electrons) are usually associated with defects introduced into semiconductor substrate during metallization by sputter deposition or electron beam deposition and during doping by ion implantation. The ions usually associated with damage during electron beam deposition are the residual vacuum gasses (such as C, N, O, H) which are ionized and then accelerated by the electric and magnetic fields in the chamber. Although there is some literature on the defects introduced during implantation [2,3], sputter deposition [4,5] and electron beam deposition [6,7] there is still lack of clear understanding of the origin and identity of some of the defects introduced by these heavy ions.

Metallization is a critical device processing step in the semiconductor industry. Resistive evaporation, electron beam deposition, and sputter deposition are commonly used metallization techniques. In this study defects introduced in n-type Ge during electron beam deposition (EBD) of different metal contacts are presented. EBD induced defects can influence device performance and alter barrier heights of the contacts. To shed more light on the origin and structure of these defects, annealing

studies were also performed. The annealing mechanism of the *E*-center is presented from which the activation energy of the annealing process is deduced.

## 9.2 Experimental Procedure

The samples used for this work were n-type, bulk grown Ge (111) doped with Sb to about  $2.5 \times 10^{15} \text{ cm}^{-3}$  and were supplied by Umicore. Before metallization the samples of 5 mm x 3 mm in size were first degreased and then etched in a mixture of  $\text{H}_2\text{O}_2$  (30%) :  $\text{H}_2\text{O}$  (1:5) for 1 minute. Immediately after cleaning they were inserted into a vacuum chamber where AuSb (0.6% Sb) was deposited by, resistive evaporation, on their back surfaces as ohmic contacts. The samples were then annealed at 350 °C in argon (Ar) for 10 minutes to minimize the contact resistivity of the ohmic contacts. Before the Schottky contact fabrication, the cleaning procedure above was repeated. Au, Ru, Pt, Ru/Au or Pt/Au contacts, 0.60 mm in diameter and 200 nm thick each were deposited by electron beam deposition. For a control sample, Au was deposited as the Schottky contact using resistive deposition. After the contact fabrication, the diodes were characterized by current – voltage (*I-V*) and capacitance – voltage (*C-V*) measurements at room temperature to determine the quality of the diodes. Defects introduced by the deposition technique were characterized by deep level transient spectroscopy (DLTS) and Laplace – DLTS (LDLTS). The ‘*signatures*’ of radiation induced defects (i.e. activation enthalpy for the electron traps and hole traps,  $E_T$ , and apparent capture cross section,  $\sigma_a$ ), were determined from Arrhenius plots of  $\ln(T^2/e)$  vs.  $1000/T$ , where ‘*e*’ is either the hole or electron emission rate, and *T* is the measurement temperature.

In order to investigate the defect annealing behaviour, the samples were annealed isochronally for 20 minutes in Ar gas from room temperature up to 500°C.

## 9.3 Published and other Results

In this section the electronic and annealing properties of defects introduced in n-type Ge by electron beam deposition are presented. The annealing behavior of these defects is investigated, with emphasis on the *E*-center (V-Sb). The annealing mechanism and activation energy of the annealing process of the *E*-center is also deduced.

### 9.3.1 Defects introduced by electron beam deposition in n-type Ge

A comprehensive discussion of defects introduced during metallization using electron beam deposition is presented in the publication at the end of section 9.3.2. A comparison has been made to defects introduced during sputter deposition and electron irradiation of similar samples.

- F.D. Auret, S.M.M. Coehlo, P.J. Janse van Rensburg, C. Nyamhere, W.E. Meyer, *Mater. Sci. in Semiconductor Processing* (2008)  
doi:10.1016/j.mssp.2008.09.001.

In addition to the results presented in the publication, other results are also presented in this section.

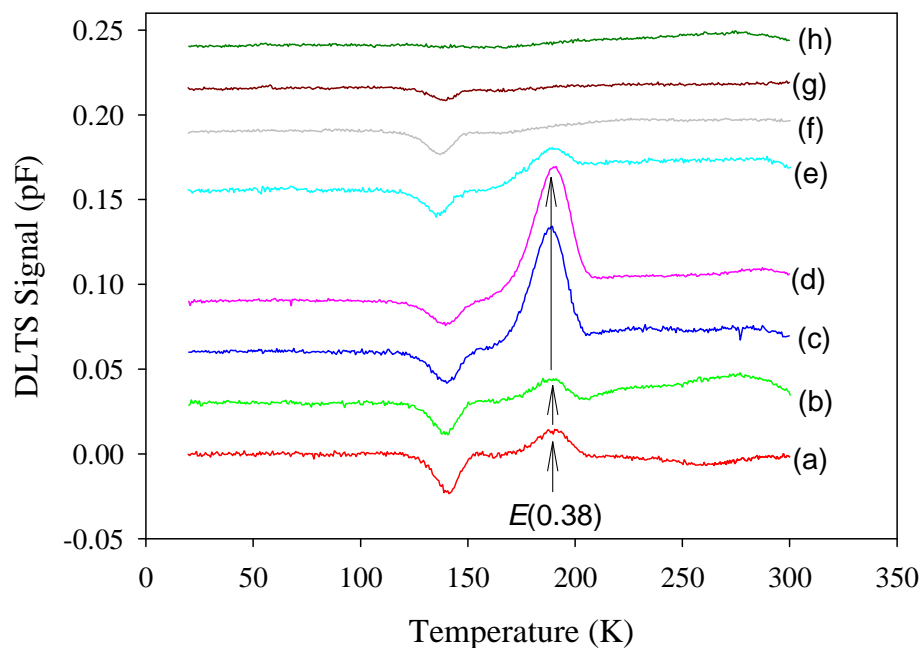


*Fig. 9-1. DLTS spectra for electron traps induced in Ge after electron beam deposition of Ru/Au Schottky contacts. The spectra were recorded (a) for as-deposited, and after annealing at (b) 100°C, (c) 150°C, (d) 175°C, (e) 200°C, (f) 225°C, (g) 250°C, (h) 300°C and (i) 350°C. These spectra were recorded with a quiescent reverse bias of -2 V, a rate window of  $80 \text{ s}^{-1}$ , a pulse voltage of -0.15 V and pulse width of 1 ms.*

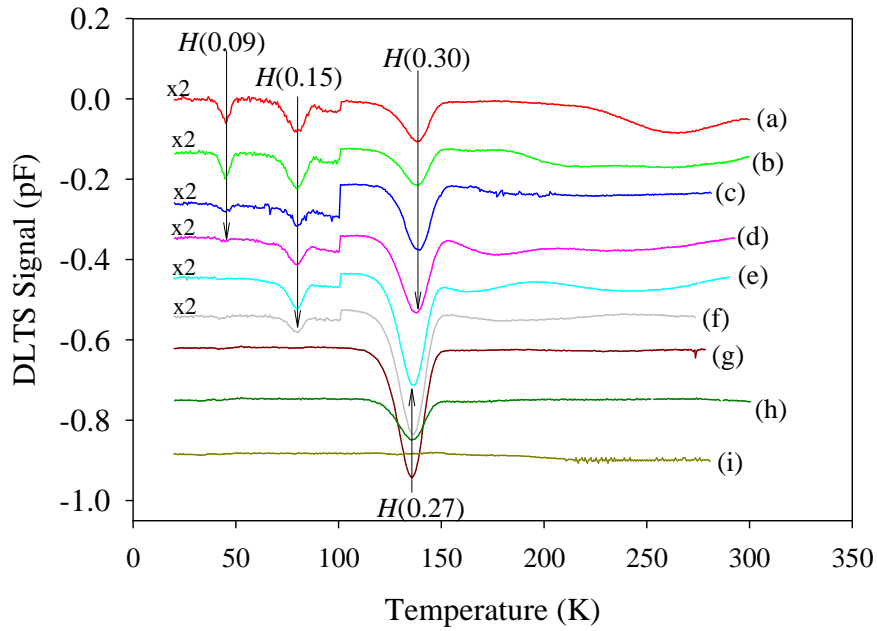


Fig. 9-2. DLTS spectra for hole traps induced in Ge after electron beam deposition of Ru/Au Schottky contacts. The spectra were recorded (a) for as-deposited, and after annealing at (b) 100°C, (c) 150°C, (d) 175°C, (e) 200°C, (f) 225°C, (g) 250°C, (h) 300°C and (i) 350°C. These spectra were recorded with a quiescent reverse bias of -1 V, a rate window of  $80 \text{ s}^{-1}$ , a pulse voltage of +3 V and pulse width of 1 ms.

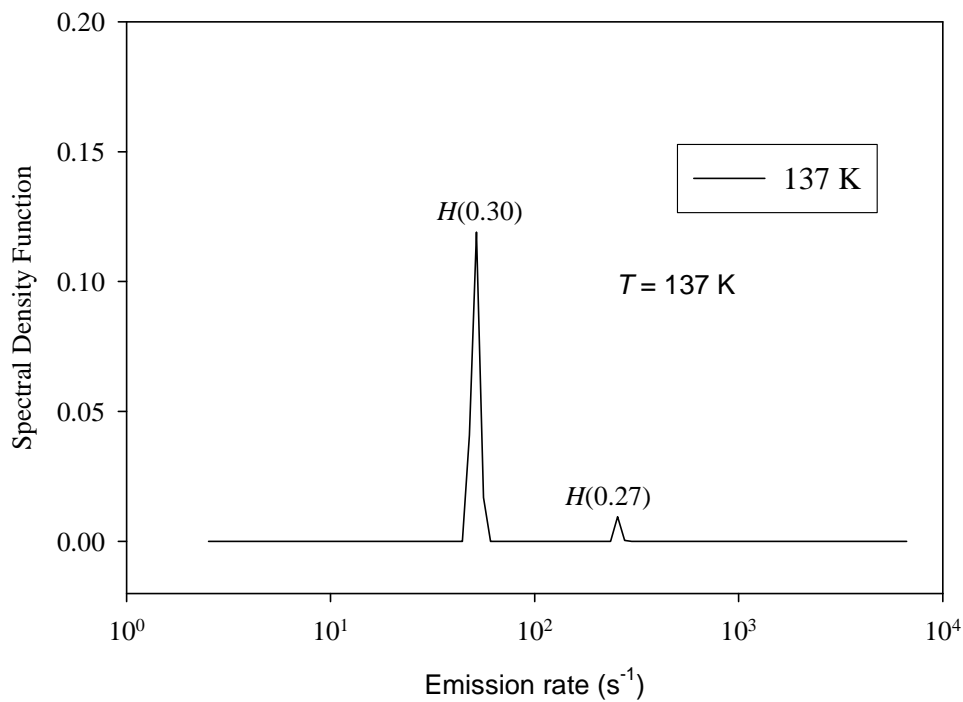


Fig. 9-3. LDLTS spectra for H(0.27) and H(0.30) in as-deposited sample recorded at 137 K.

Figs. 9-1, 9-2 and 9-3 summarize the primary defects introduced by electron beam deposition and their annealing behavior.  $E(0.38)$  level is the only detectable electron trap after Ru/Au Schottky contacts fabrication. This can be attributed to the heavy injection of minority carriers into the band gap even without applying a minority carrier filling pulse. The high barrier height formed between the Ru/Au and germanium give rise to an inversion layer close to the semiconductor surface, which is the source of these minority carriers during the application of a filling pulse. It should be noted that unlike in MeV electron irradiated samples, where the hole trap  $H(0.27)$  is introduced after annealing at  $200^{\circ}\text{C}$  or after room storage for a month, but in the case of damage introduced by EBD, this hole trap is observed immediately after the deposition. This is explained by the fact that during EBD deposition the substrate temperature is higher than the room temperature and thus thermally introducing the trap  $H(0.27)$ . The hole traps  $H(0.09)$  and  $H(0.15)$  were also observed after EBD is the (+/0) charge state of the  $E$ -center. The measurement of  $H(0.27)$  in the presence of  $H(0.30)$  was made possible by LD LTS which could clearly separate the signals as shown in Fig. 9-3. The signal of  $H(0.30)$  is much larger than that of  $H(0.27)$ , hence a much larger concentration of  $H(0.30)$  in the as-deposited samples. The concentration of  $H(0.27)$  increases with annealing temperature until it reaches a maximum at around  $225^{\circ}\text{C}$  at which point the  $E$ -center is completely removed. This reinforces the theory given in the chapter 8 that  $H(0.27)$  is a product of V-Sb after annealing to form new V-Sb<sub>2</sub> complex which is electrically active [8-9]. Although all defects were completely removed at  $350^{\circ}\text{C}$ , the annealing studies were performed up to  $600^{\circ}\text{C}$  to determine if there are any other defect levels that might be reactivated after presumably being transformed into electrical inactivate complexes during thermal annealing but no other defects were observed above  $350^{\circ}\text{C}$  annealing temperature.

### 9.3.2 Annealing mechanism of $E(0.38)$ , the $E$ -center

Since the  $E$ -center is a very important defect in Ge, for its role in (i) dopant deactivation, and free carrier removal (each V-Sb complex formation results in removal of three free carriers [10]), it is important to establish its annealing mechanism. The concentration versus depth profile of the  $E$ -center, measured at isochronal annealing temperatures between  $25^{\circ}\text{C}$  –  $175^{\circ}\text{C}$  is depicted in Fig. 9-4. The depth profile for the as-deposited sample shows that the concentration decreased from the surface of the semiconductor, which is typical of defects induced by heavy ions.

Upon annealing from 100°C up to 175°C for 20 minutes intervals, the trap showed some reverse annealing (i.e. increase in concentration with increase in annealing temperature) an indication that within this annealing temperature interval there is some unstable defect complex with vacancies as one of its constituency which dissociates and become the source of vacancy for the V-Sb center. Isochronal annealing at 175°C showed a broadened profile which shifted to lower concentrations with prolonged annealing time as depicted in Fig. 9-2, suggesting diffusion of the *E*-center during the annealing process.

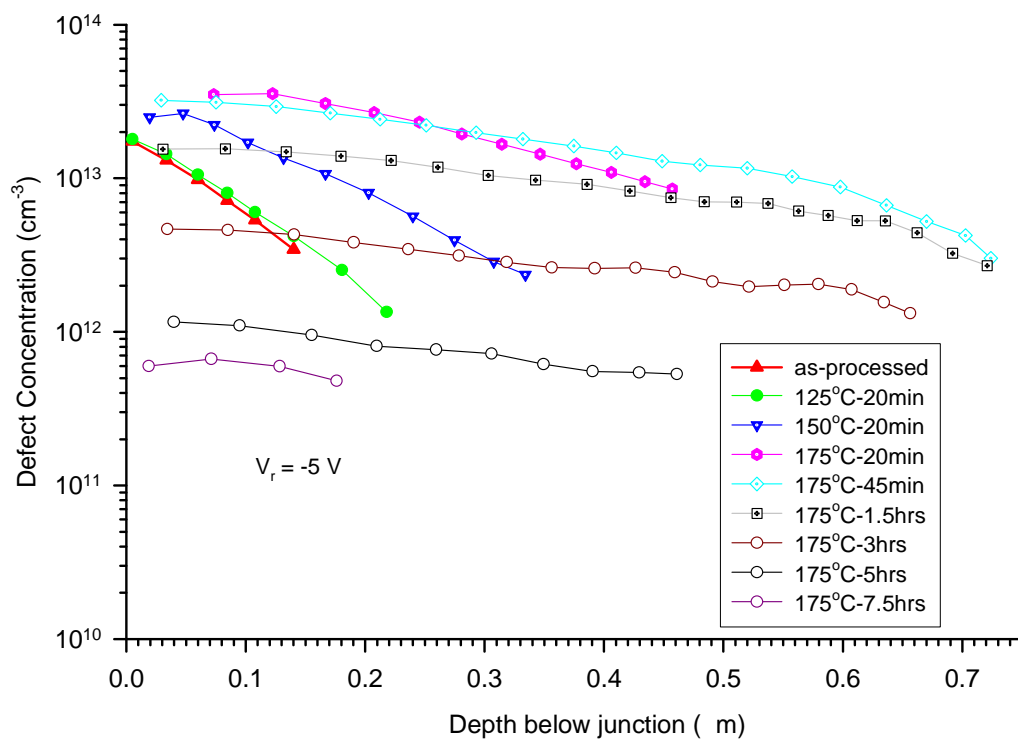


Fig. 9-4. Depth profile for *E*(0.38) recorded after annealing at different temperatures and for different period of time. The measurements were performed by LDLTS at fixed measurement temperature of 195 K, using fixed bias-variable pulse method with transition region correction [ref. 11].

Regions where vacancies are created in germanium by some of the residual vacuum gas ions (assuming a maximum energy of 10 keV for ions in the deposition chamber) are shown in the TRIM (version 2006.02) [12] simulation profiles in Fig. 9-5 (a-d). For an energy of 10 keV, the projected ion range is ~25 nm for C, N and O, each ion producing approximately 4 vacancies/nm, while H ions will create primary damage up

to a depth of  $\sim 100$  nm and each ion producing  $\sim 10 \times 10^{-3}$  vacancies/nm below the semiconductor surface.

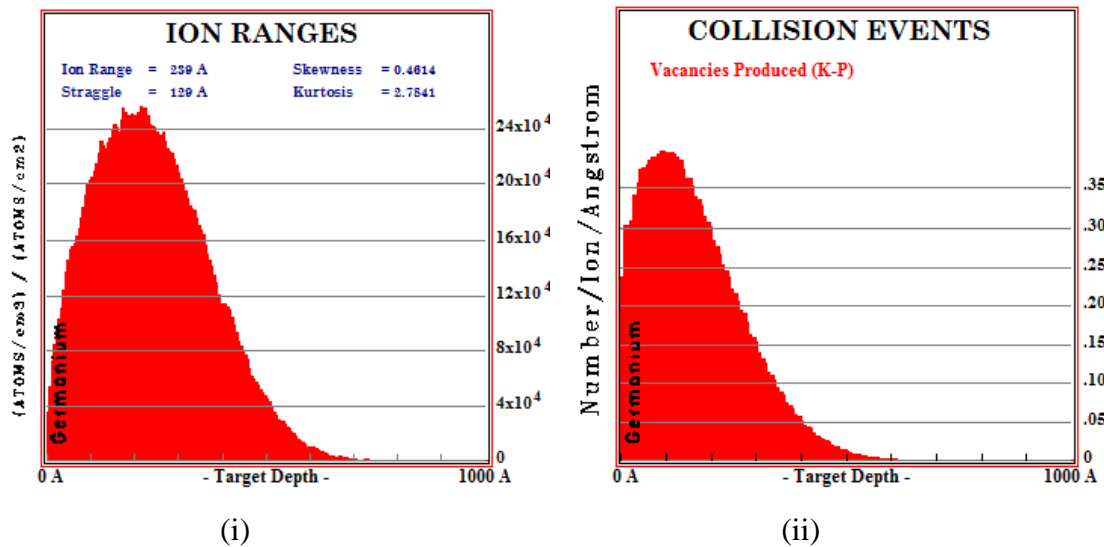


Fig. 9-5(a). (i) TRIM simulation for the projected ion range and (ii) damage events of 10 keV nitrogen ions in germanium.

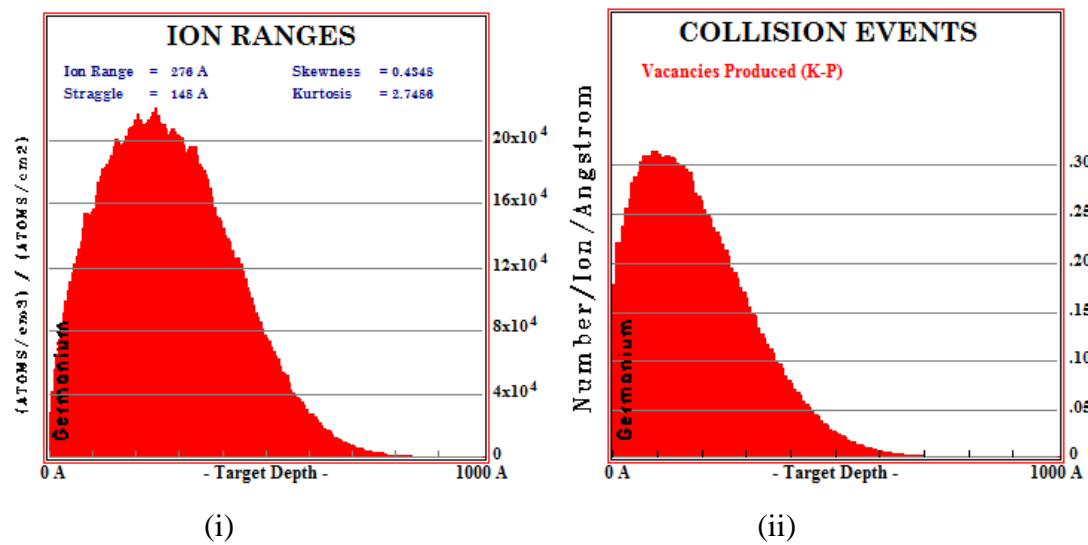


Fig. 9-5(b). (i) TRIM simulation for the projected ion range and (ii) damage events of 10 keV carbon ions in germanium.

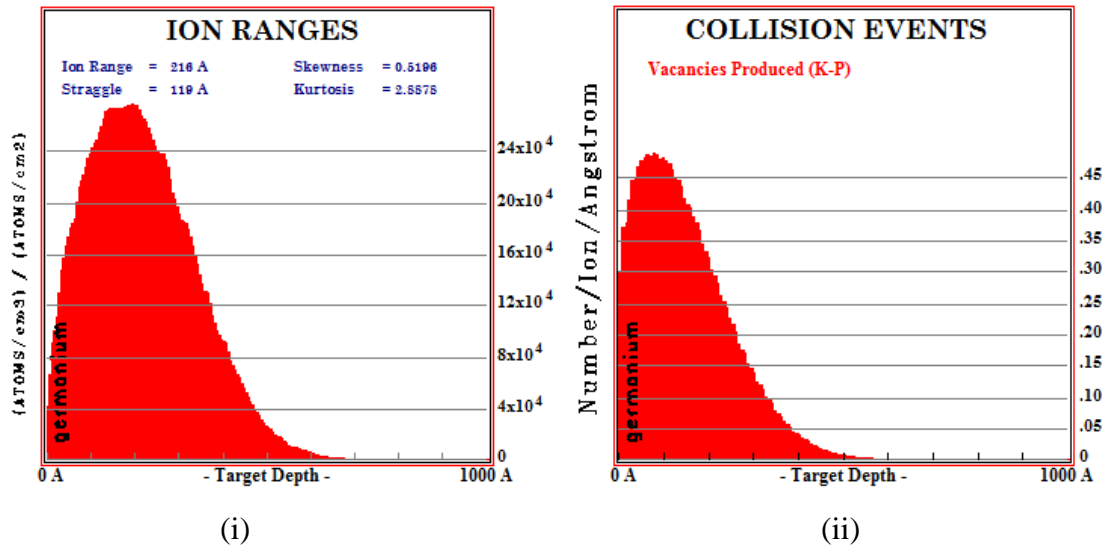


Fig. 9-5(c). (i) TRIM simulation for the projected ion range and (ii) damage events of 10 keV oxygen ions in germanium.

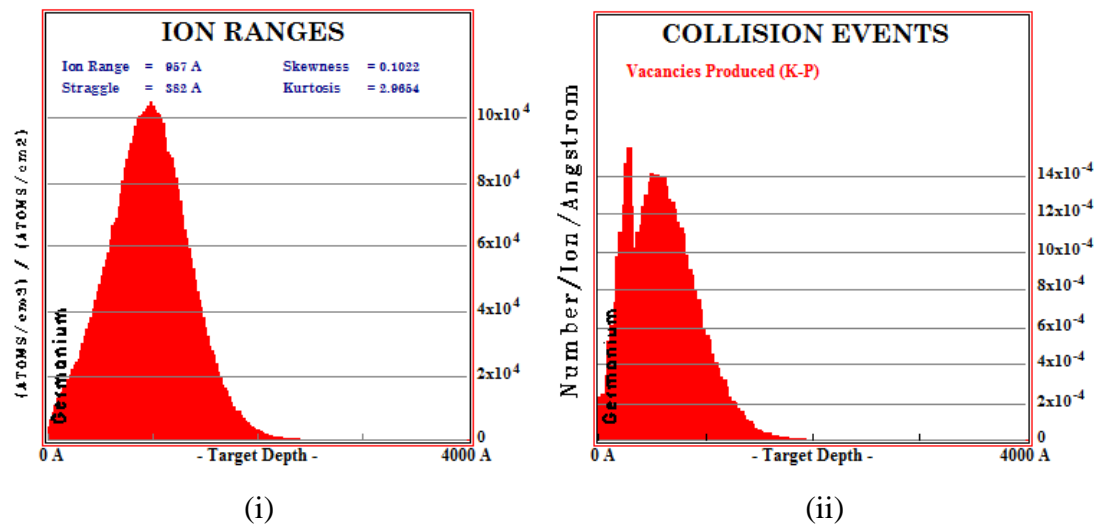


Fig. 9-5(d). (i) TRIM simulation for the projected ion range and (ii) damage events of 10 keV hydrogen ions in germanium.

This suggests that the formation of vacancy- or interstitial-related clusters is very much possible. The interstitial and vacancies created will then diffuse and form stable defect complexes (e.g. *E*-center) even deeper than the projected ion range. Thus, explaining the defect concentration profiles beyond the ion range as shown in Fig. 9-4.

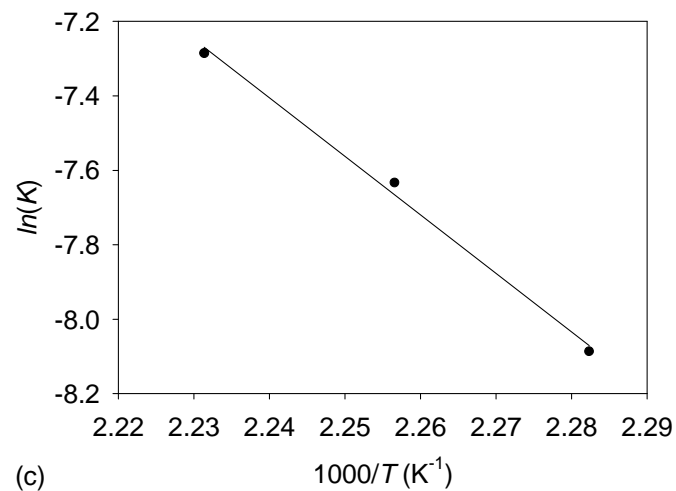
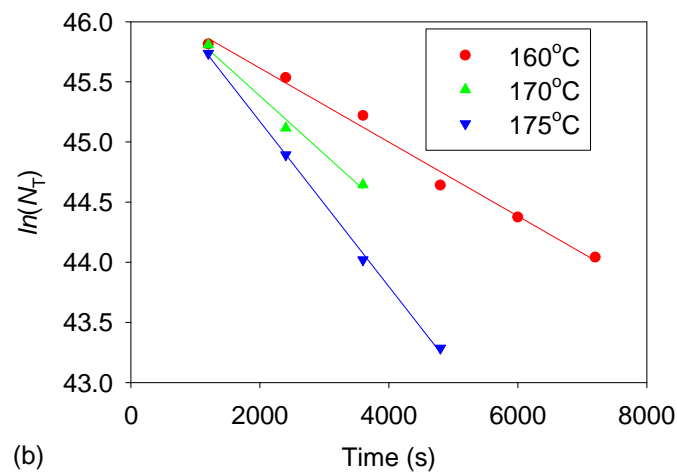
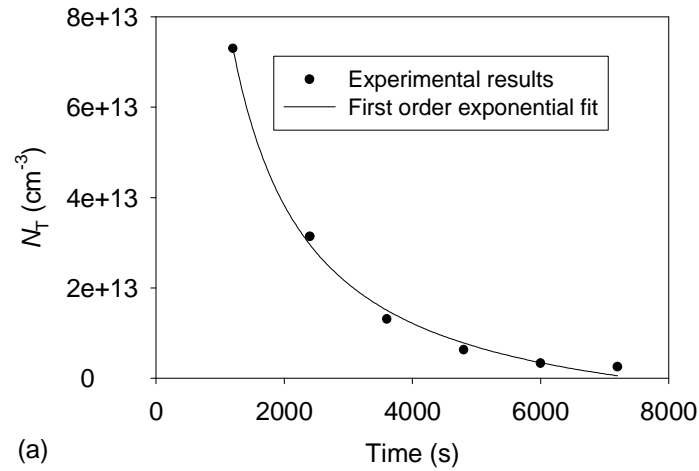


Fig. 9-6. (a) Defect concentration versus annealing time measured at annealing temperature of 175°C. The solid line represents first order exponential decay fit. (b) Semi-log plot of defect concentration profile versus annealing time measured at annealing temperatures of 160°C, 170°C and 175°C from which the annealing rate constant,  $K$ , is calculated. (c) The Arrhenius plot of  $\log(K)$  vs.  $1000/T$ .

To enhance the understanding of the annealing mechanism of the *E*-center it is important to investigate the annealing kinetics of the defect and determine the activation energy for the annealing process. The results for the annealing kinetics at temperatures 160°C, 170°C and 175°C are shown in Fig. 9-6 (b) from which the annealing rate (*K*) for each temperature (*T* in °C) was extracted and used for the construction of the Arrhenius plots depicted in graph (c). The annealing of the *E*-center follows a first order exponential decay process as shown in Fig. 9-6 (a) and (b), with an activation energy,

$$E_a = 1.36 \text{ eV}$$

and pre-exponential factor,

$$A = (1.2 \pm 0.3) \times 10^{12} \text{ s}^{-1}$$

extracted from the gradient and vertical axis intercept of the Arrhenius plot shown in Fig. 9-6(c) respectively. The value of pre-exponential factor *A*, lies just below the lower end of the purely dissociation range of  $>10^{12} \text{ s}^{-1}$  [13,14]. The value of the pre-exponential factor obtained points more to a diffusion driven annealing mechanism of the *E*-center in Ge. The annealing of the *E*-center has been associated with the introduction of the hole trap *H*(0.27) which has been attributed to higher order complex  $\text{Sb}_2\text{V}$  [15]. This has been further supported by theoretical studies by Coutinho *et al* [16], who predicted that the complex  $\text{Sb}_2\text{V}$  is an electrical active level which is close the position of V-Sb (-/0). It then follows that the *E*-center anneals by diffusing until it captures an Sb atom in the substitutional position and its structure changes to  $\text{Sb}_2\text{V}$ .



## Electrical characterization of defects introduced during metallization processes in n-type germanium

F.D. Auret\*, S.M.M. Coelho, P.J. Janse van Rensburg, C. Nyamhere, W.E. Meyer

Physics Department, University of Pretoria, Pretoria 0002, South Africa

### ARTICLE INFO

#### Keywords:

Ge  
Metallization  
Defects  
Deep-level transient spectroscopy  
DLTS

### ABSTRACT

We have studied the defects introduced in n-type Ge during electron beam deposition (EBD) and sputter deposition (SD) by deep-level transient spectroscopy (DLTS) and evaluated their influence on the rectification quality of Schottky contacts by current–voltage ( $I$ – $V$ ) measurements.  $I$ – $V$  measurements demonstrated that the quality of sputter-deposited diodes are poorer than those of diodes formed by EBD. The highest quality Schottky diodes were formed by resistive evaporation that introduced no defects in Ge. In the case of EBD of metals the main defect introduced during metallization was the V–Sb complex, also introduced during by electron irradiation. The concentrations of the EBD-induced defects depend on the metal used: metals that required a higher electron beam intensity to evaporate, e.g. Ru, resulted in larger defect concentrations than metals requiring lower electron beam intensity, e.g. Au. All the EBD-induced defects can be removed by annealing at temperatures above 325 °C. Sputter deposition introduces several electrically active defects near the surface of Ge. All these defects have also been observed after high-energy electron irradiation. However, the V–Sb centre introduced by EBD was not observed after sputter deposition. Annealing at 250 °C in Ar removed all the defects introduced during sputter deposition.

© 2008 Elsevier Ltd. All rights reserved.

### 1. Introduction

The low effective mass of holes in Ge has opened up the possibility of using Ge in ultrafast complementary metal-oxide-semiconductor (CMOS) devices [1]. This, in turn, has triggered renewed interest in the properties of defects in Ge because defects ultimately determine the performance of devices. In a detailed study of proton and electron-irradiated Ge a comparison was made to previously observed radiation-induced defects and level assignments of the E-centre (V–Sb), A-centre (V–O) and divacancy (V–V) were proposed [2]. Several other O- and Sb-related defects were characterised in O-doped and Sb-doped Ge, respectively. It was also convincingly demonstrated that the E-centre in Sb-doped Ge can be present in

three charge states and the level positions associated with these levels' states were determined [3–5].

Metallization is a critical processing step in the semiconductor industry. Resistive evaporation, electron beam deposition (EBD) and sputter deposition are commonly used metallization methods. It is well known that resistive evaporation does not introduce any detectable defects in the semiconductor. However, it cannot easily deposit high melting point materials e.g. W or Ru. EBD, on the other hand, is useful to deposit high melting point metals at very controllable rates. Sputter deposition can also be used to deposit high melting point metals and is further capable of stoichiometrically depositing alloys from compound targets. Unfortunately, these latter two methods introduce defects in semiconductors. Some investigations regarding the defects introduced in Ge during EBD [6–8] and sputter deposition [9,10] have been reported. The defects introduced during these processes reside in the Ge at and close to the metal–Ge junction;

\* Corresponding author. Tel.: +27 12 4202684; fax: +27 12 362 5288.  
E-mail address: [danie.auret@up.ac.za](mailto:danie.auret@up.ac.za) (F.D. Auret).

they influence device performance and alter the barrier heights of the contacts [11]. The defects responsible for these barrier adjustments are formed when energetic particles reach the semiconductor surface and interact with the semiconductor. Depending on the application, these defects may either be beneficial or detrimental to optimum device functioning. For Si it has been shown that the defects introduced during high-energy electron and proton irradiation increase the switching speed of devices [12].

In this study, we review the electronic properties of defects introduced in n-type Ge during EBD and sputter deposition of different metal Schottky contacts. We also show that the concentrations of the most prominent EBD-induced defect, the V-Sb centre, depended on the metal deposited by EBD via the melting point of the metal and the influence thereof on the vacuum during metallization. We have found that sputter deposition also introduces several electrically active defects near the surface of Ge, but, contrary to what has been reported elsewhere [9], it did not introduce the V-Sb centre in our experiments. Most of the defects introduced by EBD and sputter deposition have also been observed after high-energy electron irradiation. We also illustrate the effect of these process-induced defects on the current-voltage (*I*-*V*) characteristics of the Schottky diodes at different temperatures. Finally, we compare the removal of these metallization-induced defects by thermal annealing.

## 2. Experimental procedure

The Schottky barrier diodes for this study were fabricated on bulk-grown (111) n-type Ge doped with Sb to a level of  $2.5 \times 10^{15} \text{ cm}^{-3}$ . Before metallization the samples were first degreased and then etched in a mixture of  $\text{H}_2\text{O}_2:\text{H}_2\text{O}$  (1:5) for 1 min. Directly after cleaning they were inserted into a vacuum chamber where AuSb (0.6% Sb) was deposited on their back surfaces. The samples were then annealed at 350 °C in Ar for 10 min, yielding ohmic contacts with a low contact resistivity. Before Schottky contact deposition, the samples were again chemically cleaned as described above. Metal (Au, Ti and Ru) contacts, 0.6 mm in diameter and 200 nm thick, were deposited onto the Ge in an EBD system through a mechanical mask. A Varian 10 kV electron gun vacuum evaporation system was used for this process. In this system, the samples are positioned about 0.4 m above the electron gun. In a different system Au Schottky contacts were sputter deposited onto similar Ge samples cut from the same wafer. For sputter deposition Ar was leaked into the system to a pressure of  $6 \times 10^{-2}$  mbar [9]. The sputter-deposited contacts were deposited at a rate of about  $2 \text{ nm s}^{-1}$  and were 400 nm thick. "Control" Au Schottky contacts were deposited on samples cut from the same wafer by resistive evaporation.

Following contact fabrication, current-voltage (*I*-*V*) and capacitance-voltage (*C*-*V*) measurements were performed to assess the quality of the diodes and to determine the free carrier density of the Ge, respectively. Thereafter both conventional and high-resolution Laplace

deep-level transient spectroscopy (DLTS) [13,14] was used to study the defects introduced in the Ge during the EBD and SD processes. The activation energies,  $E_t$ , and apparent capture cross sections for electrons,  $\sigma_{n\sigma}$ , and holes,  $\sigma_{p\sigma}$ , (i.e. the DLTS "signatures") of the process-induced electron traps were determined from the conventional DLTS Arrhenius plots. In order to identify the defects introduced by the deposition processes, a comparison was made with defects introduced by high-energy (MeV) electron irradiation from a  $\text{Sr}^{90}$  source in samples cut from the same wafer.

## 3. Results and discussion

### 3.1. *I*-*V* characteristics of Schottky diodes fabricated by EBD and sputter deposition

*I*-*V* measurements were recorded at room temperature as well as at several other lower temperatures. The series resistances of the control diodes remained in the 10–20 Ω range in the entire temperature regime investigated, indicating that the AuSb back contacts retained their ohmic character, even down to 16 K, the lowest temperature attainable in our cryostat. Room temperature *C*-*V* measurements yielded the free carrier density of the Ge as  $(2.5 \pm 0.05) \times 10^{15} \text{ cm}^{-3}$ . In Fig. 1, we compare the forward and reverse *I*-*V* characteristics of Au Schottky contacts formed by resistive evaporation, EBD and sputter deposition at room temperature and at 100 K. We chose 100 K as

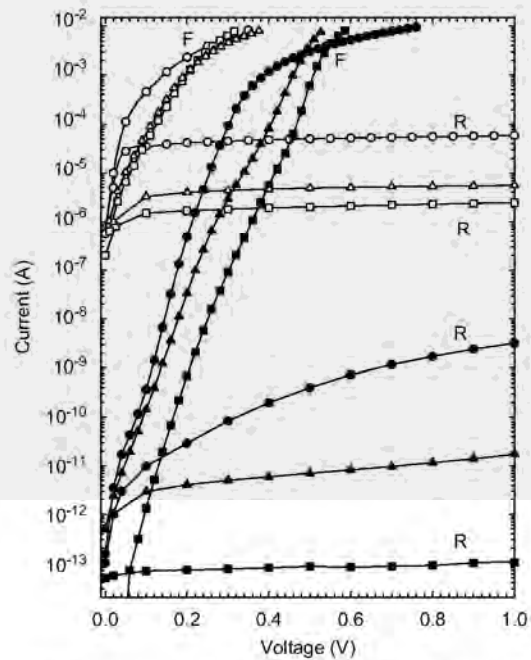


Fig. 1. *I*-*V* characteristics of Au Schottky contacts to n-Ge deposited by resistive evaporation (squares), EBD (triangles) and sputter deposition (circles). Open symbols are the data recorded at room temperature while filled symbols represent the data recorded at 100 K.

the lower temperature because at 100K the reverse leakage current of the best diodes (deposited by resistive evaporation) is between  $10^{-13}$  and  $10^{-14}$  A, which is the lowest current our equipment can accurately measure. At room temperature the  $I$ - $V$  barrier height of these three contacts were determined as  $(0.59 \pm 0.01)$ ,  $(0.56 \pm 0.01)$  and  $(0.53 \pm 0.01)$  eV, respectively.

From Fig. 1 we notice several interesting aspects. Firstly, at room temperature, the reverse leakage current of the control diodes are the best whereas that of the sputtered diodes are the poorest, by slightly more than a decade. Secondly, if we compare the characteristics of these diodes at 100K then we see that the difference between the reverse characteristics of the three diodes has been amplified. The reverse current (at  $-1$  V) of the sputter-deposited diode is more than four orders of magnitude higher than that of the control sample. The forward current characteristic of the sputter-deposited diode is also significantly higher than those of the other two diodes. These higher reverse currents may be the result of process-induced defects that act as generation centres. Another interesting point is that the forward characteristic of the sputter-deposited diode shows a significant increase in series resistance compared to the other diodes. This is especially noticeable for the characteristics recorded at 100K. This may be due to surface disorder introduced during the sputter deposition process. The control and EBD samples exhibited very similar series resistances, significantly lower than that of the sputter-deposited diode. These  $I$ - $V$  measurements clearly demonstrate that both EBD and sputter deposition resulted in degraded  $I$ - $V$  characteristics but that the sputter deposition yields the poorest diodes of the three metallization processes.

### 3.2. Defects introduced by EBD of different metals

First, we summarise what is already known for the defects introduced during EBD of Pt on Sb-doped Ge [6–8]. Note that no defects could be detected in the control SBDs fabricated by resistive deposition, indicating that the Ge is of high quality. The main defect introduced during EBD of Pt [7] was the E-centre ( $V$ -Sb complex) with its prominent associated electron and hole traps  $E_{0.38}$ ,  $H_{0.30}$  and  $H_{0.09}$ , respectively. In the nomenclature used here “E” means electron trap and the number following it is the energy level of this trap below the conduction band. Similarly, “H” means hole trap and the number following it is the energy level of this trap above the valence band. Note that we have not corrected these energy values to take into account the temperature dependence of the capture cross section, which has been shown to significantly change the activation energy of the E-centre [3]. Several other electron traps in lower concentrations were also detected. In the case of EBD the E-centre forms when energetic particles (originating in the region of the filament) impinge on the Ge and create vacancies at and close to the Ge surface [15]. These vacancies are mobile at room temperature and migrate into the Ge where they combine with Sb-dopant atoms to form the E-centre.

In Fig. 2, we compare the DLTS results recorded using SBDs of three different metals, namely Ti, Au and Ru, formed by EBD. The top three curves ((a)–(c)) are for electron traps but clearly hole injection could not be completely eliminated and therefore they still show the  $H_{0.30}$  trap. The lower three curves ((d)–(f)) are for hole traps and were obtained after using intentional hole injection. As was the case for Pd and Pt, the most significant defect introduced is the E-centre with the traps  $E_{0.38}$ ,  $H_{0.30}$  and  $H_{0.09}$  associated with it [3–8]. Curve (b) also shows the presence of a defect  $E_{0.13}$  in a lower concentration, whereas curves (e) and (f) reveal the presence of additional hole traps,  $H_{0.15}$  and  $H_{0.18}$ . The DLTS signatures of these defects were extracted from the Arrhenius plot in Fig. 3 and are summarised in Table 1.

From Fig. 2 it is further evident that the concentration of the E-centre increases from Ti to Au to Ru. In order to explain this trend, it should be borne in mind that the defects introduced by EBD are caused by ionised particles that are accelerated from the region near the filament [15] and impinge on the Ge surface. The concentration of these particles in the residual gas in the vacuum will increase with increasing residual gas pressure as well as with increasing emission current (proportional to the filament current). In the case of Ti evaporation, the starting vacuum

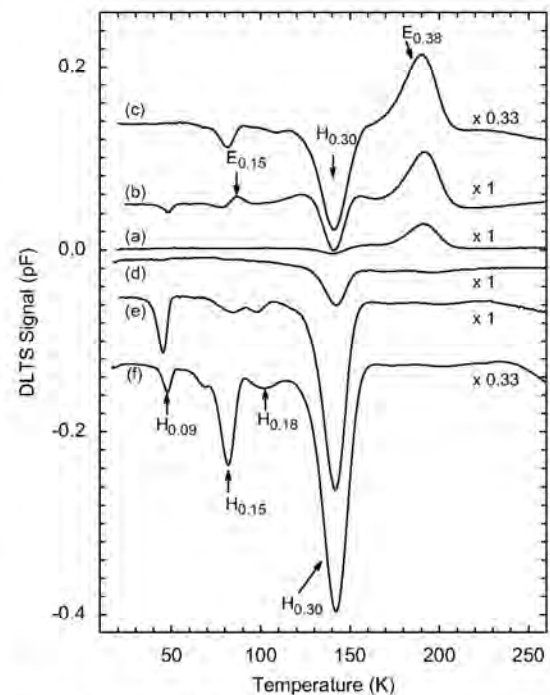


**Fig. 2.** DLTS spectra of Ti, Au and Ru Schottky contacts deposited by EBD to n-Ge: Curves (a), (b) and (c) are the electron-trap spectra for Ti, Au and Ru, respectively, while curves (d), (e) and (f) are the hole-trap spectra for Ti, Au and Ru, respectively. These spectra were recorded using a rate window of  $80 \text{ s}^{-1}$  at a quiescent reverse bias of  $-1$  V. For the electron-trap spectra the pulse,  $V_p$ , was  $0.15$  V into forward bias. Hole-trap spectra were obtained by applying an injection pulse of  $V_p = 3$  V into forward bias.

was more than an order of magnitude lower than for Au and Ru (Table 2). This means that, although the filament current was slightly higher than for Au deposition, a lower flux of particles reached the sample surface during

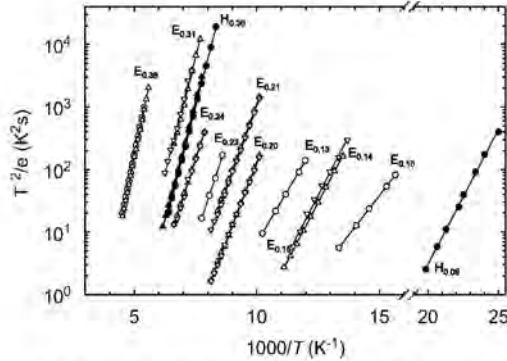


**Fig. 3.** Arrhenius plots for defects introduced by EBD (circles), MeV electron irradiation induced (triangles up) and sputter deposition (triangles down) in Ge. Filled symbols are for hole traps. All data were acquired using the bias and pulsing conditions defined in the caption of Fig. 2.

evaporation, which in turn implies a lower level of damage, as observed in Figs. 1 and 2. When comparing the conditions for Au and Ru it can be seen from Table 2 that the vacuum during Au deposition was about the same as for Ru deposition. The filament current for Au deposition was only slightly lower than for Ru. However, if we consider the deposition rates then we notice that, due to its high melting point, the deposition rate of Ru is about one-twentieth of that of Au. This implies that it takes 20 times longer to deposit the same thickness of Ru as Au. This in turn means that the Ge surface is exposed to energetic particles for a much longer time during Ru deposition than during Au deposition, leading to the high concentration of defects observed for Ru metallization.

### 3.3. Comparison of defects introduced by EBD and sputter deposition

Curves (b) and (c) in Fig. 4 represent the DLTS spectra for Au Schottky diodes that were deposited by sputter deposition and EBD, respectively. Curve (d) was recorded after irradiating a resistively deposited diode with high-energy electrons at a dose of  $2 \times 10^{14} \text{ cm}^{-2}$ . We have used Laplace DLTS to separate the signals of the  $E_{0.20}$  and  $E_{0.21}$

**Table 1**

Electronic properties of prominent defects introduced in n-type Ge during sputter and electron beam deposition of Schottky contacts, and by MeV electron irradiation

| Sputter deposition              |                           |   |                         | MeV electron irradiation |              |                              |                         | Similar defects/defect ID                               |
|---------------------------------|---------------------------|---|-------------------------|--------------------------|--------------|------------------------------|-------------------------|---|
| Defect                          | $E_T$ (eV) ( $\pm 0.01$ ) | $\sigma_d$ ( $\text{cm}^2$ ) ( $\pm 10\%$ ) | $T_{\text{peak}}^a$ (K) | Defect                   | $E_T$ (eV)   | $\sigma_d$ ( $\text{cm}^2$ ) | $T_{\text{peak}}^a$ (K) |   |
| $ES_{0.14}$                     | $E_C - 0.14$              | $5.5 \times 10^{-15}$                       | 78                      | $E_{0.15}$               | $E_C - 0.15$ | $2.8 \times 10^{-14}$        | 77                      | $E_{0.13}^b$ , Sb and I related <sup>c</sup>            |
| $ES_{0.20}$                     | $E_C - 0.20$              | $3.7 \times 10^{-14}$                       | 100                     | $E_{0.20}$               | $E_C - 0.20$ | $1.4 \times 10^{-14}$        | 100                     | $E_{0.19}^c$ , Sb and I related <sup>d</sup>            |
| $ES_{0.21}$                     | $E_C - 0.21$              | $2.0 \times 10^{-14}$                       | 109                     | $E_{0.21}$               | $E_C - 0.21$ | $3.6 \times 10^{-14}$        | 109                     | $E_{0.21}^c$ , Sb related <sup>e</sup>                  |
| $ES_{0.24}$                     | $E_C - 0.24$              | $3.3 \times 10^{-15}$                       | 131                     | $E_{0.24}$               | $E_C - 0.24$ | $2.5 \times 10^{-15}$        | 131                     | $E_{0.23}^c$ , Sb and I related <sup>f</sup>            |
| $ES_{0.31}$                     | $E_C - 0.31$              | $1.5 \times 10^{-14}$                       | 151                     | $E_{0.31}$               | $E_C - 0.31$ | $5.0 \times 10^{-14}$        | 150                     | $E_{0.29}^g$ , $V_2^g$                                  |
| <b>Electron beam deposition</b> |                           |   |                         |                          |              |                              |                         |   |
| $E_{0.10}$                      | $E_C - 0.10$              | $3.7 \times 10^{-16}$                       | 65                      |                          |              |                              |                         |   |
| $E_{0.13}$                      | $E_C - 0.13$              | $1.9 \times 10^{-16}$                       | 85                      |                          |              |                              |                         |   |
| $E_{0.23}$                      | $E_C - 0.23$              | $3.4 \times 10^{-14}$                       | 116                     |                          |              |                              |                         |   |
| $E_{0.38}$                      | $E_C - 0.38$              | $1.0 \times 10^{-14}$                       | 191                     | $E_{0.38}$               | $E_C - 0.38$ | $1.1 \times 10^{-14}$        | 191                     | $E_{0.37}^b$ , $E_{0.37}^c$ , V-Sb (-/-) <sup>h,c</sup> |
| $H_{0.09}$                      | $E_V + 0.09$              | $2.1 \times 10^{-13}$                       | 47                      |                          |              |                              |                         |   |
| $H_{0.15}$                      | $E_V + 0.15$              | $7.1 \times 10^{-14}$                       | 82                      |                          |              |                              |                         |   |
| $H_{0.18}$                      | $E_V + 0.18$              | $3.5 \times 10^{-14}$                       | 97                      |                          |              |                              |                         |   |
| $H_{0.27}$                      | $E_V + 0.27$              | $2.4 \times 10^{-13}$                       | 133                     |                          |              |                              |                         |   |
| $H_{0.30}$                      | $E_V + 0.30$              | $6.2 \times 10^{-13}$                       | 141                     | $H_{0.30}$               | $E_V + 0.30$ | $3.66 \times 10^{-13}$       | 142                     | $H_{0.307}^b$ , $H_{0.30}^c$ , V-Sb (-/0) <sup>h</sup>  |

The error margins the value of  $E_T$  lie in the third digit after the decimal point whereas that for  $\sigma$  is less than 10% of its value.

<sup>a</sup> Peak temperature at a rate window of  $80 \text{ s}^{-1}$ .

<sup>b</sup> See Ref. [3].

<sup>c</sup> See Ref. [2].

**Table 2**

Electron beam deposition parameters and conditions for different metal Schottky contacts

| Metal | Melting point ( $^{\circ}\text{C}$ ) | Thickness (nm) | Deposition rate (nm/s) | EB filament current (mA) | Starting vacuum (mbar) |
|-------|--------------------------------------|----------------|------------------------|--------------------------|------------------------|
| Ti    | 1660                                 | 100            | 0.4                    | 75                       | $2 \times 10^{-6}$     |
| Au    | 1064                                 | 200            | 0.5                    | 60                       | $5 \times 10^{-5}$     |
| Ru    | 2250                                 | 50             | 0.02                   | 70                       | $6 \times 10^{-5}$     |

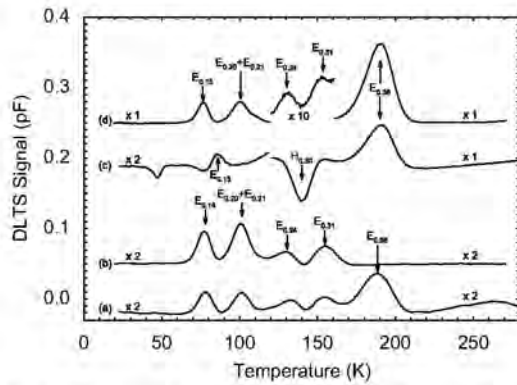


**Fig. 4.** DLTS spectra of Au Schottky contacts on n-Ge: Curves (a), (b) and (c) are the spectra for a sputter-deposited Au contact, a Au contact deposited by EBD and an electron-irradiated control contact, respectively. These spectra were recorded using a rate window of  $80\text{ s}^{-1}$  at a quiescent reverse bias of  $-1\text{ V}$ . For the electron-trap spectra the pulse,  $V_p$ , was  $0.15\text{ V}$  into forward bias.

of electron-irradiated samples. As described above, the E-centre is the only defect that is introduced by both EBD and high-energy electron irradiation. Curve (b) shows that sputter deposition introduced several electron traps:  $E_{0.14}$ ,  $E_{0.20}$ ,  $E_{0.21}$ ,  $E_{0.24}$  and  $E_{0.31}$ . However, the main electron trap introduced by EBD and electron irradiation, the E-centre, is not present in sputter-deposited diodes. Also, unlike in previous studies of high-energy electron-irradiated Ge and electron beam-deposited (EBD) Schottky diodes [6,7], we could not detect any hole traps in the sputter-deposited contacts studied here, even when applying a strong forward bias. However, after irradiating the sputter-deposited contacts with MeV electrons the  $E_{0.38}$  trap associated with the E-centre could be clearly observed (curve (a) of Fig. 4). This means that sputter deposition by itself, in our sputter equipment and under our deposition conditions, does not introduce the E-centre. It is important to point out that the E-centre has been observed by Simoen et al. [10] after sputter deposition of Pt in a different sputter system.

The fact that the E-centre is not observed after sputter deposition in our system may imply that our sputter process does not introduce a sufficient number of single vacancies at and close to the surface that can diffuse into the Ge and combine with Sb ions to form V-Sb, as in the case of EBD. It should be realised that most of the damage that we observe after sputter deposition is caused by backscattered neutral Ar ions that, for the sputter conditions used here, have a maximum energy of approximately  $700\text{ eV}$  of RF power [9]. From TRIM [14] modelling we have found that the range and straggle of these ions are  $2.1$  and  $1.2\text{ nm}$ , respectively. In the first  $3\text{ nm}$  each ion deposits on average  $20\text{ eV/nm}$  in to the Ge lattice and produces, on average,  $5$  vacancies/nm. This implies that defects larger than the single vacancy, e.g. divacancy and vacancy or interstitial clusters, can be formed. Whereas vacancy clusters, such as the divacancy, are stable at room temperature [2], interstitial clusters, by nature, are not very

stable. It is therefore conceivable that when they break up, interstitials are injected into the Ge during sputter deposition. Based on this we speculate that the defects we observe after sputter deposition are related to interstitial-impurity complexes (e.g. I-Sb) or vacancy or interstitial clusters, or complexes of these clusters with impurities. The signature of  $E_{0.31}$  is close to that reported for the divacancy ( $E_{0.29}$ ) [2], whereas the signatures of  $E_{0.14}$ ,  $E_{0.20}$  and  $E_{0.21}$  are close to that of the  $E_{0.13}$ ,  $E_{0.19}$  and  $E_{0.23}$  proposed to be related to Sb and the Ge interstitial [2].

### 3.4. Annealing of the metallization-induced defects

We have previously investigated the thermal stability of the defects introduced by EBD of Pt contacts by isochronal annealing in argon (Fig. 5) [7]. Only after annealing at  $225\text{ }^\circ\text{C}$  could the  $E_{0.38}$  and  $H_{0.30}$  levels no longer be detected. This is slightly higher than the  $175\text{--}200\text{ }^\circ\text{C}$  reported in Ref. [3] for removing the E-centre. However, it should be borne in mind that the annealing in Ref. [3] was under zero bias where most of the E-centres are filled with electrons. In our case, although we annealed at zero bias, the E-centres are very close to the surface and hence the levels of most of them are above the Fermi level. It has been reported that reverse bias annealing (E-centre level above the Fermi level) impedes the annealing of E-centres [2]. During annealing the concentration of  $H_{0.26}$  increased up to  $200\text{--}225\text{ }^\circ\text{C}$ , rendering it the most prominent defect, and then it annealed out at  $350\text{ }^\circ\text{C}$ . At this temperature all the defects introduced during EBD were removed.

We have also previously investigated the thermal stability of the defects introduced by sputter deposition of Au contacts by isochronal annealing in argon [9]. After annealing at  $150\text{ }^\circ\text{C}$  the  $E_{0.14}$ ,  $E_{0.20}$  and  $E_{0.24}$  levels could no longer be detected but the concentration of  $E_{0.31}$  increased by about a factor of two. Annealing at  $200\text{ }^\circ\text{C}$  reduced the

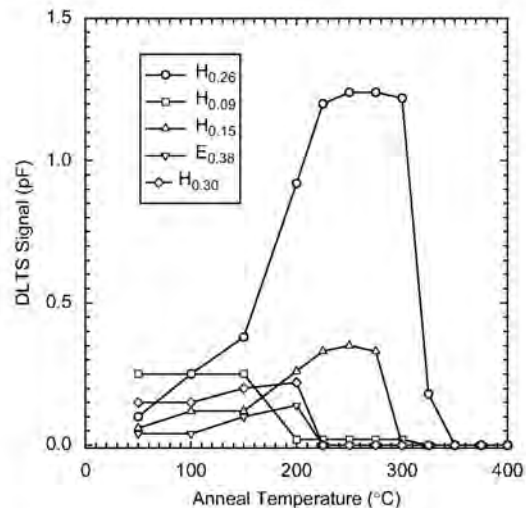


**Fig. 5.** Isochronal annealing (20 min periods) of the most prominent defects introduced by EBD in n-Ge [8].

concentrations of  $E_{0.21}$  and  $E_{0.31}$  by 10% and 30%, respectively, and annealing at 250 °C removed these defects completely, and no sputter deposition-induced defects could be detected any more. After annealing at 300 °C, no additional defects, i.e. no “second generation” defects could be observed, indicating that the sputter-deposition-induced defects did not reconstruct during annealing to form larger defects or different defect complexes.

#### 4. Summary and conclusions

The  $I$ – $V$  measurements demonstrated that both EBD and sputter deposition resulted in degraded  $I$ – $V$  characteristics, but that sputter deposition yields the poorest diodes of the two metallization methods. The higher forward and reverse currents of Au Schottky contacts formed by sputter deposition and EBD as compared to resistively deposited Au contacts is most probably the result of process-induced defects that act as generation centres. Also, the sputter-deposited diode shows a significant increase in series resistance compared to the other diodes. This may be due to surface disorder introduced during the sputter deposition process.

Our DLTS results revealed that the main defect introduced during EBD has the same electronic properties as that of the V–Sb complex, or E-centre, introduced during high-energy electron irradiation of Ge. EBD also introduced several defects that are not introduced by electron irradiation, speculated to be higher-order vacancy clusters and complexes thereof with impurities. We show that the concentrations of the most prominent EBD-induced defect, the V–Sb centre, depended on the metal deposited by EBD via the melting point of the metal and the influence thereof on the vacuum during metallization: in general, low melting point metals resulted in less EBD damage. All the defects introduced by sputter deposition have also been observed after high-energy electron irradiation, but the V–Sb complex was not observed after sputter deposition. Annealing at 350 and 250 °C in Ar removed the defects introduced during EBD and sputter deposition, respectively, and annealing at higher temperatures did not introduce any new defects.

The role of these electron beam deposition and radiation-induced defects in optimising device performance for specific applications of Ge diodes will have to be carefully examined in order to ensure optimum device performance.

#### Acknowledgements

The authors gratefully acknowledge financial support of the South African National Research Foundation. The Laplace DLTS software and hardware used in the research was kindly provided by A.R. Peaker (Centre for Electronic Materials Devices and Nanostructures, University of Manchester) and L. Dobaczewski (Institute of Physics, Polish Academy of Sciences).

#### References

- [1] Germanium silicon: physics and materials. In: Hull R, Bean JC, editors. Semiconductors and semimetals, vol. 56. San Diego: Academic Press; 1999.
- [2] Fage-Pedersen J, Nylandsted Larsen A, Mesli A. Phys Rev B 2000;62(10):116.
- [3] Markevich VP, Peaker AR, Litvinov VV, Emstev VV, Murin LI. J Appl Phys 2004;95:4078.
- [4] Markevich VP, Hawkins ID, Peaker AR, Emstev KV, Emstev VV, Litvinov VV, et al. Phys Rev B 2004;70:235213–21.
- [5] Markevich VP, Hawkins ID, Peaker AR, Litvinov VV, Dobaczewski L, Lindström JL. Appl Phys Lett 2002;81:1821.
- [6] Auret FD, Meyer WE, Coelho SMM, Hayes M. Appl Phys Lett 2006;88:242110.
- [7] Auret FD, Meyer WE, Coelho SMM, Hayes M, Nel JM. Mater Sci Semiconductor Process 2006;9:576–9.
- [8] Auret FD, Coelho SMM, Hayes M, Meyer WE, Nel JM. Phys Status Solidi (a) 2008;205(1):159–61.
- [9] Auret FD, Coelho S, Meyer WE, Nyamhere C, Hayes M, Nel JM. J Electron Mater 2007;36(12):1604.
- [10] Simoen E, Opsomer K, Claeys C, Maex K, Detavernier C, Van Meirhaegh RL, et al. Appl Phys Lett 2006;89:202114.
- [11] Myburg G, Auret FD. J Appl Phys 1992;71:6172.
- [12] Sawko DC, Bartko J. IEEE Nucl Sci 1983;30:1756.
- [13] Dobaczewski L, Kaczor P, Hawkins ID, Peaker AR. J Appl Phys 1994;76:194.
- [14] Dobaczewski L, Peaker AR, Bonde Nielsen K. J Appl Phys 2004;96:4689.
- [15] Christensen C, Petersen JW, Nylandsted Larsen A. Appl Phys Lett 1992;61:1426.

## 9.4 Summary and conclusions

Similar to defects induced by electron irradiation, DLTS and LDLS revealed that the dominant defect introduced by electron beam deposition is the V-Sb (*E*-center). This shows that during electron beam deposition vacancies are created below the semiconductor surface by particles which are ionized around the filament and then accelerated by the magnetic and electric fields towards the sample. EBD also introduced some defects which were not observed in the electron irradiated samples. The concentration of V-Sb depended on the type of metal deposited via the melting point of the metal and the influence thereof on the vacuum during metallization. In general, low melting point metals resulted in less EBD damage. The *E*-center is removed after annealing at 225°C, which is slight higher than the temperature at which this defect anneals in the electron irradiated samples. This difference in the annealing temperature has been attributed to the fact that the *E*-centers in the EBD deposited samples are closer to the surface and hence most of them are empty of electrons and this has been observed to impede the annealing of the *E*-center, whereas in the electron irradiated samples the *E*-center is deeper and hence most of the centers are filled with electrons during the annealing process. A hole trap *H*(0.27) exhibits some reverse annealing between from room temperature and reaches maximum concentration at 225°C and anneals out at 350°C. This trap has been attributed to the V-Sb<sub>2</sub> complex. All the defects were completely removed after annealing at 350°C, which is a low thermal budget when compared to defects in silicon. This shows that defects in germanium have relatively lower binding energies than in silicon.

The annealing mechanism of the *E*-center has been investigated and it was found that it anneals by first order process with an activation energy 1.36 eV, and pre-exponential factor of  $(1.2 \pm 0.3) \times 10^{12} \text{ s}^{-1}$ . Therefore, it is proposed that the *E*-center in Ge anneals by diffusion until its structure changes to another electrical active complex V-Sb<sub>2</sub>.

## References

- 
- [1] M. Lannoo, J. Bourngoïn, *Point Defects in Semiconductors I, Theoretical Aspect* Springer series in solid state science 22, (1981).
- [2] F.D. Auret, P.J. Janse van Rensburg, M. Hayes, J.M. Nel and W.E. Meyer, *Appl. Phys. Lett.* **89**, (2006) 152123.
- [3] A.R. Peaker, V.P. Markevich, B. Hamilton, I.D. Hawkins, J. Slotte, K. Kuitunen, F. Tuomisto, A. Satta, E. Simoen and N.V. Abrosimov, *Thin Solid Films* **517** (2008) 152.
- [4] F.D. Auret, S. Coehlo, W.E. Meyer, C. Nyamhere, M. Hayes and J.M. Nel, *J. of Electronic Materials* Vol. **36 No.2**, (2007) 1604.
- [5] E. Simoen, K. Opsomer, C. Claeys, K. Maex, C. Detavernier and R.L van Meirhaegh, *Appl. Phys. Lett.* 89 (2006) 202114.
- [6] F.D. Auret, W.E. Meyer, S. Coehlo and M. Hayes, *Appl. Phys. Lett.* **88**, (2006) 242110.
- [7] F.D. Auret, S.M.M. Coehlo, P.J. Janse van Rensberg, C. Nyamhere and W.E. Meyer, *Mater. Sci. in Semiconductor Processing* (2008) doi:10.1016/j.mssp.2008.09.001.
- [8] V.P. Markevich, S. Bernardini, I.D. Hawkins, A.R. Peaker, V.I. Kolkovskiy, A. Nylandsted Larsen and L. Dobaczewski, *Mater. Sci. in Semiconductor Processing* (2008) doi:10.1016/j.mssp.2008.09.007.
- [9] J. Coutinho, V.J.B. Torres, S. Öberg, A. Carvalho, C. Janke, R. Jones *et al*, *Mater. Sci. Mater. Electron* **18** (2007) 769.
- [10] V.P. Makervich, A.R. Peaker, V.V. Litvinov, V.V. Emstev and L.I. Murin, *J. Appl. Phys.* **95**, 4078 (2004).
- [11] Y. Zohta and M.O. Watanabe, *J. Appl. Phys.* **53** No.3 (1982) 1809.
- [12] J.P. Biersack and L.G. Hagmark, *Nucl. Instrum. Methods* **174** (1980) 257.
- [13] M. Mikelsen, E.V. Monakhov, G. Alfieri, B.S. Avset and B.G. Svensson, *Phys. Rev. B* 72 (2005) 195207.
- [14] F.D. Auret and P.N.K. Deenapanray, *Crit. Rev in Solid State and Mater. Sci.* 29 (2004) 1.
- [15] V.P. Markevich, *Mater. Sci. in Semicond. Process.* **9** (2006) 589.
- [16] J. Coutinho, V.J.B. Torres, S. Öberg, A. Carvalho, C. Jonke, R. Jones and P.R. Briddon, *J. Mater. Sci.: Mater. Electron.* **18** (2007) 769.

## List of publications

1. F.D. Auret, S.M.M. Coehlo, P.J. Janse van Rensburg, C. Nyamhere and W.E. Meyer Mater. Sci. in Semiconductor Processing (2008)  
doi:10.1016/j.mssp.2008.09.001.
2. F.D. Auret, S. Coehlo, W.E. Meyer, C. Nyamhere, M. Hayes and J.M. Nel, J. of Electronic Materials Vol. **36 No.2**, (2007) 1604.

# Chapter 10

## Defects introduced in antimony-doped germanium after sputtering by 3 keV Ar ions

### 10.1 Introduction

It is generally believed that heavy low energy ions may create shallow complex defects when compared to electrons and protons. Sputter deposition [1,2] and electron beam deposition [3,4] are associated with heavy ion damage in semiconductors. Sputtering is a widely used metal deposition and surface cleaning technique in microelectronics and generally is associated with defect creation by low energy heavy ions [3,4]. Aggressive scaling has resulted in the need for shallow junctions [5]. Defects introduced by low energy ions (e.g. during sputter etching) are usually located close to the semiconductor surface and therefore are important, particularly for shallow junction devices, as they will determine the reliability and performance of these devices. In this chapter defect levels introduced by low energy (3 keV) argon (Ar) ions are characterized.

### 10.2 Experimental Procedure

We have used bulk grown *n*-type Ge with (111) crystal orientation, doped with antimony, (Sb) to a density of  $2.6 \times 10^{15} \text{ cm}^{-3}$  supplied by Umicore. Before metallization the samples of 0.5 cm x 0.3 cm in size were first degreased and then etched in a mixture of H<sub>2</sub>O<sub>2</sub> (30%) : H<sub>2</sub>O (1:5) for 1 minute. Immediately after cleaning they were placed in a vacuum chamber where AuSb (0.6% Sb), 130 nm thick, was deposited by resistive evaporation on their back surfaces as ohmic contacts. The samples were then annealed at 350 °C in argon (Ar) for 10 minutes to optimize the ohmic contacts. Prior to the Schottky contact fabrication, the samples were sputtered by 3 keV Ar ions of fluences,  $1 \times 10^{13} \text{ cm}^{-2}$  and  $1 \times 10^{14} \text{ cm}^{-2}$  using the

sputter gun in an Auger electron spectroscopy (AES) system. The sputtering process resulted in approximately 500 Å, thick layer being removed. Immediately after sputtering, Pd contacts, 0.60 mm in diameter and 100 nm thick were deposited by vacuum resistive evaporation. After the contacts were formed, the samples were characterized by current – voltage ( $I$ - $V$ ) and capacitance – voltage ( $C$ - $V$ ) techniques at room temperature. The defects introduced were characterised by DLTS and Laplace – DLTS [6,7]. The ‘*signatures*’ of radiation induced defects (i.e. activation enthalpy for the electron and hole traps  $E_T$ , and apparent capture cross section,  $\sigma_a$ ), were determined from Arrhenius plots of  $\log(T^2/e)$  vs.  $1000/T$ , where ‘ $e$ ’ is either the hole or electron emission rate, and  $T$  is the measurement temperature.

DLTS measurements were performed regularly over a period of 4 months to monitor defect stability and evolution at room temperature. To obtain more information on the defects introduced by Ar ions sputtering, the samples were then annealed isochronally for 20 minutes in Ar gas from room temperature up to 300°C. After each and every annealing cycle,  $I$ - $V$ ,  $C$ - $V$ , DLTS and LDLTS measurements were performed.

### 10.3 Results

In this section the electronic and annealing properties of electron and hole traps created by Ar sputtering are discussed. The room temperature stability of the primary defects is also investigated.

#### 10.3.1 Defects introduced in Ge after electron irradiation with different doses

The DLTS spectra (Fig. 10-1) shows the finger prints of the hole traps recorded after 3 keV sputtering with Ar ions of fluence  $1 \times 10^{14} \text{ cm}^{-2}$ . Fig. 10-1 curve (a) shows the spectra recorded immediately after irradiation and curve (b) shows the spectra after one month of room temperature storage. The DLTS spectra measured immediately after the sputtering reveals an electron trap level  $E(0.38)$  and two hole traps  $H(0.09)$  and  $H(0.31)$  curve (a). In this nomenclature ‘ $E$ ’ is the electron trap and ‘0.38’ is the position of the trap from the conduction band whereas ‘ $H$ ’ is the hole trap and ‘0.09’ is the position of the trap relative to the valence band. After room temperature annealing for about a month a hole trap  $H(0.26)$  was observed. It should be noted that

the un-sputtered Ge did not contain any defects in the detectable range limit, which is consistent with data in refs. [8-9].

Table. 10.1. The summary of electron properties of primary defects introduced by 3 keV Ar sputter damage in n-Ge and secondary defects introduced after thermal annealing.

| Defect    | $E_T$ (eV)   | $\sigma_a$ (cm <sup>2</sup> ) | $T^a_{\text{peak}}$ (°C) | $T^b_{\text{in}}$ (°C) | $T^c_{\text{out}}$ (°C) | Defect Origin        |
|-----------|--------------|-------------------------------|--------------------------|------------------------|-------------------------|----------------------|
| $E(0.38)$ | $E_C - 0.38$ | $5.1 \times 10^{-14}$         | 191                      | RT                     | 225                     | V-Sb (--/-) [3,8-11] |
| $H(0.09)$ | $E_V + 0.09$ | $7.8 \times 10^{-13}$         | 45                       | RT                     | 225                     | V-Sb(+/0) [10]       |
| $H(0.14)$ | $E_V + 0.14$ | $1.3 \times 10^{-14}$         | 77                       | 50                     | 275                     | $H_{0.15}$ [3,4]     |
| $H(0.26)$ | $E_V + 0.26$ | $1.8 \times 10^{-13}$         | 140                      | RT                     | 200                     | ?                    |
| $H(0.27)$ | $E_V + 0.27$ | $5.1 \times 10^{-13}$         | 140                      | 200                    | ---                     | V-Sb <sub>2</sub> ?  |
| $H(0.30)$ | $E_V + 0.30$ | $7.3 \times 10^{-14}$         | 142                      | 200                    | ---                     | ?                    |
| $H(0.31)$ | $E_V + 0.31$ | $3.3 \times 10^{-14}$         | 142                      | RT                     | 225                     | V-Sb (0/-) [3,8-11]  |
| $H(0.40)$ | $E_V + 0.40$ | $4.8 \times 10^{-11}$         | 150                      | 200                    | ---                     | ?                    |

<sup>a</sup>Peak temperature with a rate window of 80 s<sup>-1</sup>. <sup>b</sup>Temperature at which the defect was introduced. <sup>c</sup> Temperature at which the defect was removed.

The defect ‘signatures’ of the radiation induced defects and those that evolved at room temperature were extracted from the Arrhenius plots, shown in Fig. 10-5 (filled circles) and the electron properties of these traps are summarised in Table 10.1. When compared with defects introduced in similar samples by 1 MeV electron irradiation [8-11,12], sputter deposition [1,2] and electron beam deposition [3,4],  $H(0.09)$ ,  $H(0.31)$  and  $E(0.38)$  have also been observed in the electron irradiated samples and electron beam deposition [3,4,13].  $H(0.09)$ ,  $H(0.31)$  and  $E(0.38)$  have been assigned to the (+/0), (0/-), (--/-) charge states of the  $E$ -center respectively [3,8-11]. The identity of  $H(0.26)$  is not clear at the moment.

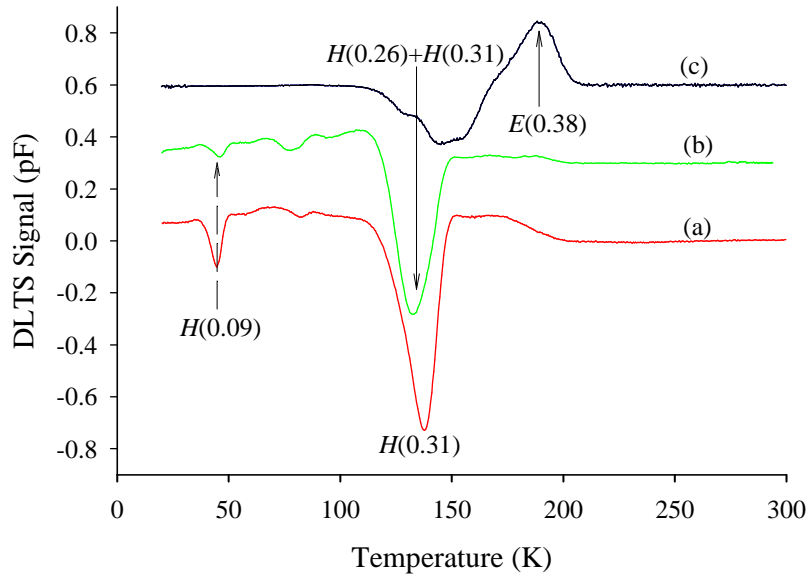


Fig. 10-1. The DLTS hole spectra after 3 keV Ar ions sputtering with a fluence of  $1 \times 10^{14} \text{ cm}^{-2}$ , on n-Ge, (a) immediately after sputtering and (b) after room temperature annealing for a month. (c) DLTS electron traps spectra after sputtering. These spectra were recorded at a rate window (RW) of  $80 \text{ s}^{-1}$ , a quiescent reverse bias of  $V_r = -2 \text{ V}$  with a filling pulse  $V_P = +3 \text{ V}$  (hole traps) and  $V_P = 0 \text{ V}$  (electron traps) superimposed on the reverse bias and with a pulse width of 1 ms.

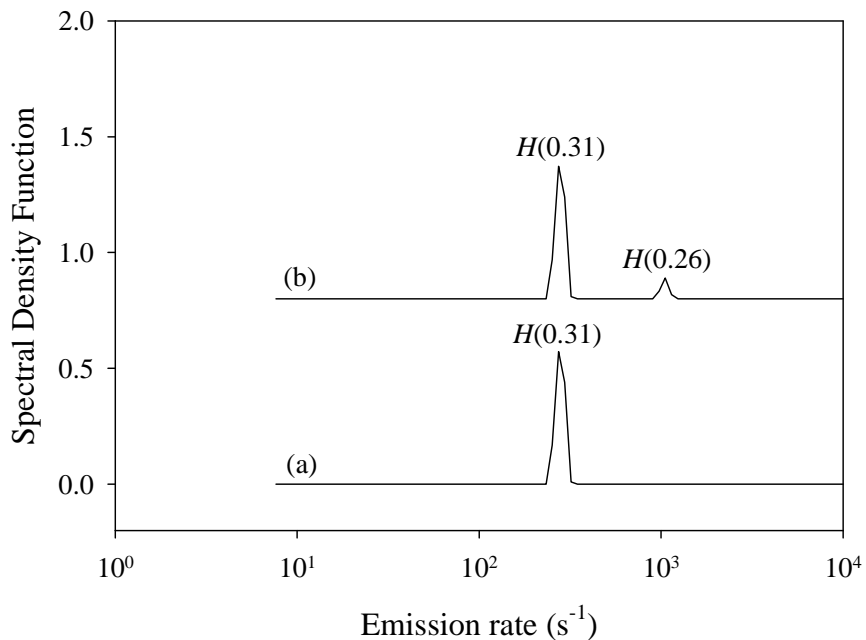


Fig. 10-2. LDLTS spectra recorded (a) immediately after sputtering showing H(0.31) peak and (b) after room storage for a month showing peaks for both H(0.31) and H(0.26). Both spectra were recorded at a temperature of 143 K.

The DLTS depicts a single sharp peak immediately after the sputtering process attributed to the  $H(0.31)$  as shown in Fig. 10-2 (a) and after a month at room temperature another peak for trap  $H(0.26)$  emerges on DLTS spectra as clearly illustrated in Fig. 10-2 (b), resulting in an apparently DLTS single peak slightly shifted to lower temperature.

### 10.3.2 Annealing behavior of the electron and hole traps

The annealing behavior of defects induced by 3 keV Ar ions sputtering on Ge is depicted in Fig. 10.3 and the electron properties extracted from the annealing graphs and Arrhenius plots depicted in Fig. 10-6 (open circles, after annealing at 225°C) and (open triangles, after annealing at 275°C) are summarized in Table. 10.1. The hole traps  $H(0.09)$ ,  $H(0.26)$ ,  $H(0.31)$  and  $E(0.38)$  were stable up to 175°C as shown in Figs. 10-3 and 10.5 but  $H(0.09)$  and  $H(0.31)$  were both removed after annealing at 225°C.

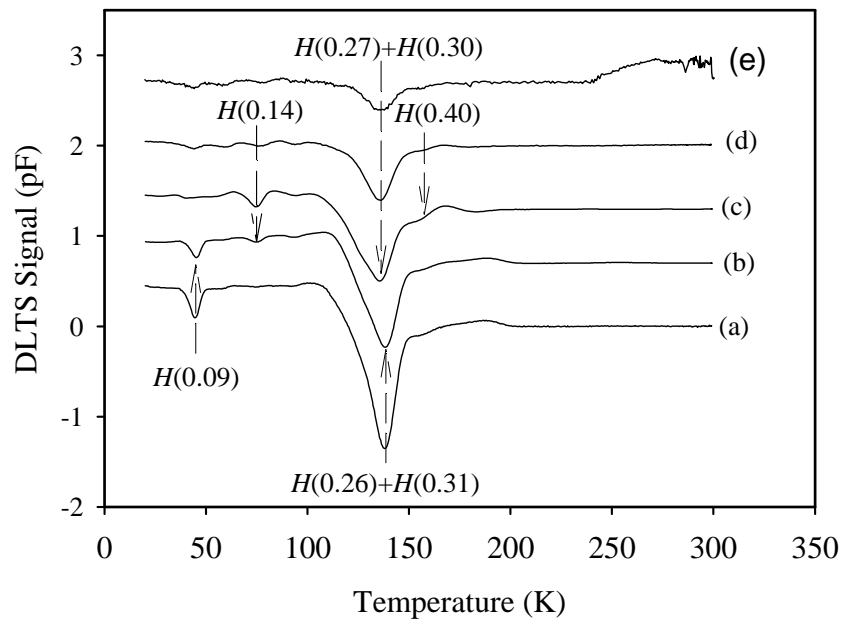


Fig. 10-3. The DLTS spectra showing defects created in  $n$ -Ge doped with Sb after sputtering with 3 keV Ar ions of fluence  $1 \times 10^{14} \text{ cm}^{-2}$  (a) after room temperature annealing for a month, and after annealing at (b) 175°C, (c) 225°C, (d) 250°C, (e) 285°C. The measurements were recorded at quiescent reverse bias,  $V_r = -2$  V, pulse voltage,  $V_p = +3$  V, pulse width of 1 ms and rate window (RW) of  $80 \text{ s}^{-1}$ .

The hole trap  $H(0.14)$  was introduced after annealing at  $50^\circ\text{C}$  and was removed at  $275^\circ\text{C}$  whereas traps  $H(0.27)$ ,  $H(0.30)$  and  $H(0.40)$  are observed after annealing at  $225^\circ\text{C}$  and were still present at the highest annealing temperature of  $285^\circ\text{C}$  beyond which the diodes were too degraded for DLTS measurements. The Arrhenius plots in Fig. 10-6 clearly shows that the pair  $H(0.27)$  and  $H(0.26)$  and the pair  $H(0.30)$  and  $H(0.31)$  are indeed different sets of defects.

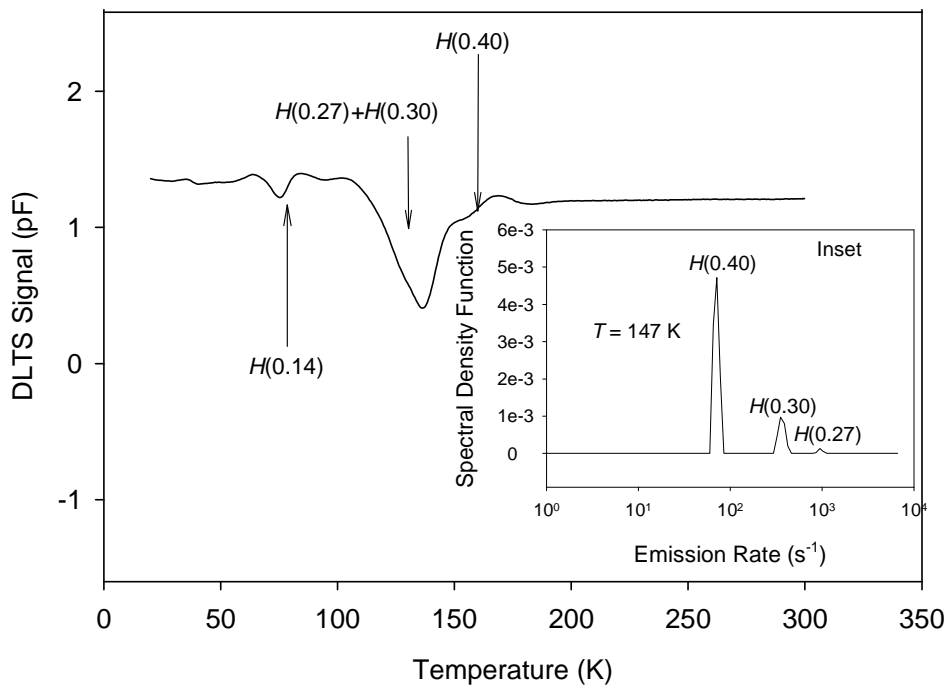


Fig. 10-4. DLTS spectra recorded after annealing at  $225^\circ\text{C}$ . Inset: LDLTS showing the peaks  $H(0.27)$ ,  $H(0.30)$  and  $H(0.40)$  measured at  $147\text{ K}$ .

$H(0.27)$  has been observed after electron beam deposition and has been attributed to  $\text{V-Sb}_2$  complex since it is observed after the annealing of the  $E$ -center [14].  $H(0.30)$  and  $H(0.40)$  are new secondary defects and their identities are still unclear at the moment, but could be attributed to higher order  $\text{V}_n\text{-Sb}_n$  complexes. LDLTS was successfully used to separate the trap levels  $H(0.27)$ ,  $H(0.30)$  and  $H(0.40)$  as shown in Fig. 10-4 (inset). Annealing studies of similar samples irradiated with electrons [8-11] and after electron beam deposition [3-4] did not reveal the same secondary defects suggesting that introduction of these complex defects are dependent on the mass and energy of the irradiating particles.

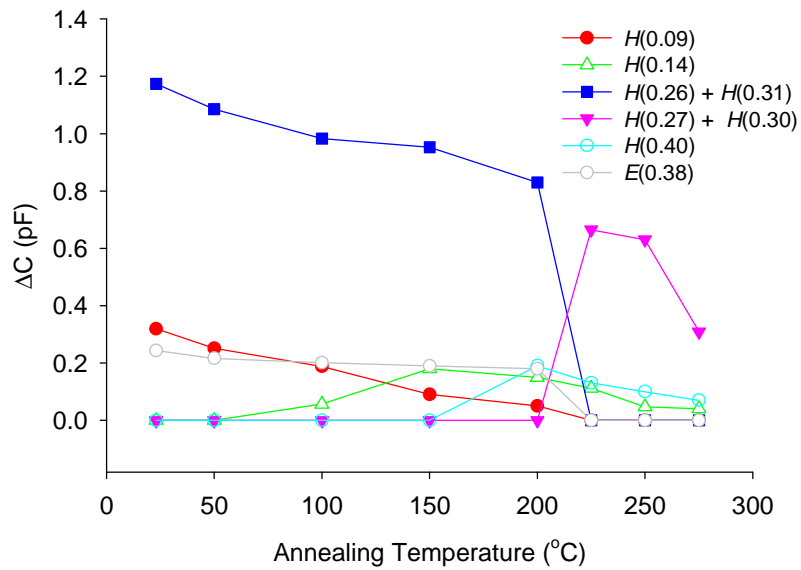


Fig. 10-5. Annealing behavior of defects introduced in germanium by 3 keV Ar sputtering.

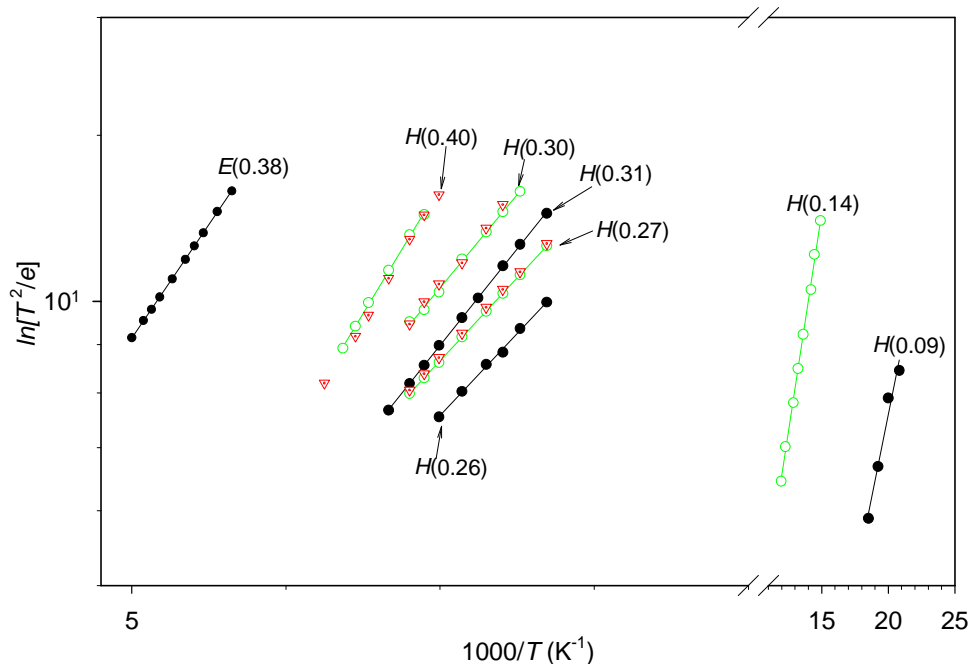


Fig. 10-6. The Arrhenius plots of the defects created in n-Ge after 3 keV sputtering with Ar ions with a dose of  $1 \times 10^{14} \text{ cm}^{-2}$  for as-sputtered and recorded after a month (solid black circles), after annealing at 225°C (open green circles) and after annealing at 275°C (open red triangles).

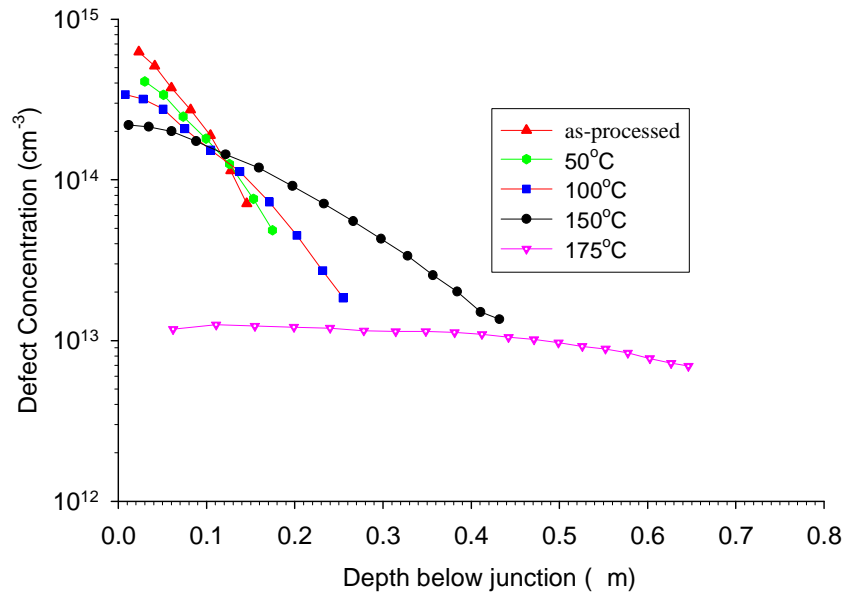


Fig. 10-7. Defect depth profile for the E(0.38) (E-center) recorded at various isothermal annealing temperatures from room temperature upto 175°C.

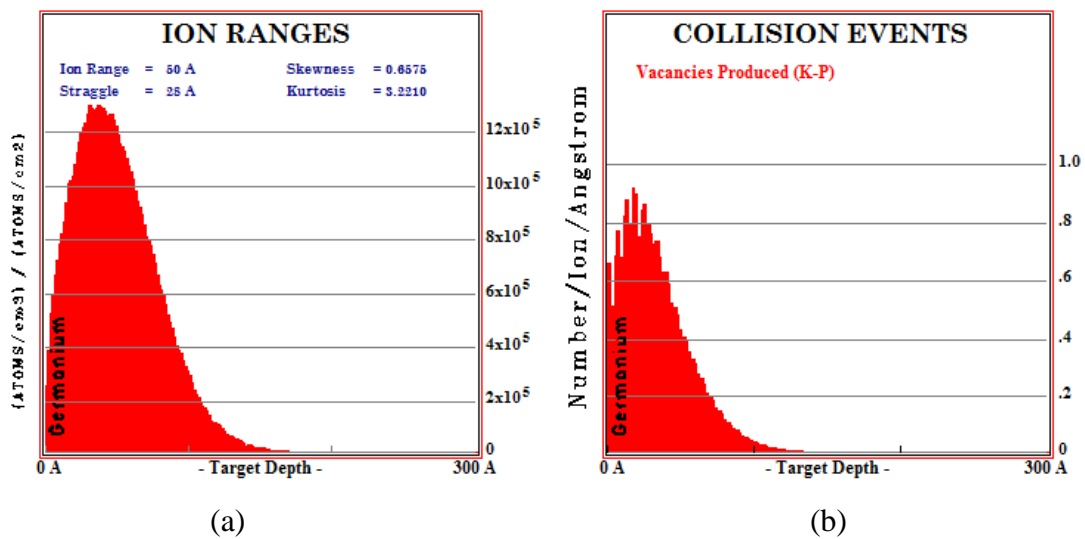


Fig. 10-8. (a) TRIM simulation for the projected ion range and (b) damage events of 3 keV argon ions in germanium.

The depth profile of the E-center for as-irradiated samples showed a decrease in concentration from the semiconductor surface, which is a characteristic of damage by heavy ions as shown in Fig. 10-7. Upon annealing, the profile broadened and defect concentration significantly decreased at a temperature of 175°C, which indicates the diffusion of the traps deeper into the material before its structure changes at 225°C.

The projected ion range of the Ar ions in germanium is 5 nm below the junction and each ion produces, on average, 9 vacancies/nm as shown in the TRIM (version 2006.02) [15] simulation depicted in Fig. 10-8. The vacancy-interstitial pairs are expected to be formed within this projected ion range region before they diffuse and captured by other impurities to form stable complexes. Thus, higher order vacancy- or interstitial-related complex defects are likely to be formed.

#### 10.4 Summary and conclusions

The 3 keV Ar ion sputtering introduces three primary traps,  $H(0.09)$ ,  $H(0.31)$ , and  $E(0.38)$  which are similar to those introduced by electron irradiation and electron beam deposition which are the single donor, single acceptor and double acceptor charge state of the  $E$ -center respectively. The trap  $E(0.38)$  is the only electron trap observable after the sputtering process and the observation of other electron traps could have been impeded by injection of minority carrier even without applying minority carrier injection pulse. The creation of the V-Sb center shows that Ar sputtering introduces vacancy-interstitial pairs at and below the semiconductor surface. After room temperature storage for a month, a trap  $H(0.26)$  was observed and the origin of this trap is still not clear at the moment. The annealing studies have further revealed hole traps  $H(0.27)$ ,  $H(0.30)$  and  $H(0.40)$  which were all formed after the annealing of the  $E$ -center at 200°C.  $H(0.27)$  has been observed after electron irradiation and annealing and also after electron beam deposition. It has been suggested that this center is a product of the  $E$ -center annealing and has been assigned to V-Sb<sub>2</sub>.  $H(0.30)$  and  $H(0.40)$  have not been observed before and their identities are still unknown at the moment, but be higher order, vacancy- or interstitial-related complexes. More work in terms of defect models are required to identify these secondary defects.

## References

- 
- [1] F.D. Auret, S. Coehlo, W.E. Meyer, C. Nyamhere, M. Hayes and J.M. Nel, *J. of Electronic Materials*, Vol. **36 No.2**, (2007) 1604.
- [2] E. Simoen, K. Opsomer, C. Claeys, K. Maex, C. Detavernier and R.L. van Meirhaegh, *Appl. Phys. Lett.* **89** (2006) 202114.
- [3] F.D. Auret, W.E. Meyer, S. Coehlo and M. Hayes, *Appl. Phys. Lett.* **88**, (2006) 242110.
- [4] F.D. Auret, W.E. Meyer, S. Coehlo and M. Hayes, J.M. Nel, *Mater. Sci. Semiconductor Process*, **9**, (2006) 576.
- [5] L.D. Yau, *Solid State Electronics*, vol. **17**, (1974) 1059.
- [6] L. Dobaczewski, P. Kaczor, I.D. Hawkins, A.R. Peaker, *J. Appl. Phys.* **76** (1994) 194.
- [7] L. Dobaczewski, A.R. Peaker and K.B. Nielsen, *J. Appl. Phys.* **96** (2004) 4689.
- [8] J. Fage-Pedersen, A. Nylandsted Larsen and A. Mesli, *Phys. Rev. B.* **62** (2000) 10116.
- [9] Cloud Nyamhere, F.D. Auret, A.G.M. Das and A. Chawanda, *Physica B* **401-402** (2007) 499.
- [10] C.E. Lindberg, J. Lundsgaard Hansem, P. Bomholt, A. Mesli, K. Bonde-Nielsen and A. Nylandsted Larsen, *Appl. Phys. Lett.* **87** (2005) 172103.
- [11] Cloud Nyamhere, M. Das, F.D. Auret and A. Chawanda, *Phys. Stat. Sol. (C)* **5 No. 2** (2008) 623.
- [12] F.D. Auret, S. Coelho, W.E. Meyer, C. Nyamhere, M. Hayes and J.M. Nel, *J. of Electronic Mater.* **36 No.2** (2007) 1604.
- [13] F.D. Auret, S.M.M. Coehlo, P.J. Janse van Rensberg, C. Nyamhere and W.E. Meyer, *Mater. Sci. in Semiconductor Processing* (2008), doi:10.1016/j.mssp.2008.09.001.
- [14] V.P. Markevich, S. Bernardini, I.D. Hawkins, A.R. Peaker, V.I. Kolkovsky, A. Nylandsted Larsen and L. Dobaczewski, *Mater. Sci. in Semiconductor Processing* (2008) doi:10.1016/j.mssp.2008.09.007.
- [15] J.P. Biersack and L.G. Haggmark, *Nucl. Instrum. Methods* **174** (1980) 257.



## List of Publications

C. Nyamhere, A.G.M. Das, F.D. Auret, A. Chawanda, W. Mtangi, Q. Odendaal and A. Carr, *Physica B*. doi:10.1016/j.physb.2009.09.037.

# Chapter 11

## Conclusions

Detailed conclusions for specific experimental results have been presented at the end of each and every chapter. In this chapter a more general summary is presented.

Deep level transient spectroscopy (DLTS) and Laplace-DLTS (LDLTS) have been used successfully to characterize defects introduced in silicon and germanium by MeV electron irradiation and during metallization by electron beam deposition. LDLTS has been particularly useful in the deconvolution of deep levels with similar emission rates ( $e_1/e_2 > 2$ ), which otherwise could not be resolved by DLTS. New defect levels have been observed by using high resolution LDLTS which were not observed before by DLTS, enhancing the understanding of radiation and process-induced defects in silicon and germanium.

It has been shown that defects are introduced at and below the semiconductor surface during metallization. The source of the damage has been attributed to the residual vacuum gases, such as carbon, nitrogen, and oxygen, which are ionized near the filament region and then accelerated by magnetic and electric fields towards the sample, thereby causing lattice damage in the substrate region close to the surface. The vacancies and interstitial created are mobile at room temperature, hence they diffuse until they are captured by other impurities to form stable complexes.

Defects introduced in n- and p-type silicon by electron irradiation and during electron beam deposition have been characterized and compared. Although there are several similar defects, electron beam deposition introduces other defects which were not observed after electron irradiation. The reason for this lies in the nature of primary

damage introduced by irradiating particles. Heavier ions create vacancy-rich regions along the ion path with interstitial-rich regions near the end of projectile. Therefore, the opportunity for multi-vacancy and multi-interstitials reactions are much greater leading in complex defect formation. On the other hand, light particles such as, electrons, create uniform distribution of Frenkel pairs along their path, resulting in simple vacancy and interstitial-related defects uniformly distributed with the material.

Similarly, defects introduced in n-type germanium by both MeV electron irradiation and during electron beam deposition have been characterized and compared. The most dominant defect observed after the two processes is the V-Sb (*E*-center). This shows that the energetic particles found in the electron beam deposition and electron irradiation introduces vacancy-interstitial pairs beneath the semiconductor surface, which will then diffuse and form stable vacancy-related and other defects. Detailed annealing studies on the *E*-center showed an activation energy of 1.36 eV for the annealing process and a pre-exponential of  $(1.2 \pm 0.3) \times 10^{12} \text{ s}^{-1}$  and this point to a diffusion-driven annealing mechanism of this center. It is worth noting that while the divacancy in silicon is well known and has been characterized, in germanium this trap level has not been identified by experimental techniques.

In contrast to silicon, all electron irradiation and electron beam deposition damage were removed easily from germanium with very low thermal budget of between 350°C - 400°C compared to a thermal budget between 500°C - 600°C for defects in silicon. The annealing thermal budget indicates relative lower binding energies of defects in germanium than in silicon.

Although defects introduced in silicon and germanium have been characterized in this work, in terms of defect signatures and annealing properties, some of these defects are still to be identified. Thus, more work, in terms of defect models is necessary to properly identify these defects.

### **Future work**

Further work can be done to characterize defects introduced during low energy (keV range) sputtering using other noble gas ions such as, Ne, Kr, Xe. The energy and fluences of the noble gas ions can also be varied.

More research work is required to identify the residual vacuum particles which are responsible for the lattice damage on and beneath the samples surfaces during electron beam deposition. Various modification to the EBD system maybe done, e.g. putting a shield around the sample to limit or eliminate damage from residual gas particles.